ELSEVIER

Transient Natural Convection Heat Transfer to Starch Dispersion in a Cylindrical Container: Numerical Solution and Experiment

W. H. Yang & M. A. Rao*

Department of Food Science and Technology, Cornell University-Geneva,
Geneva, NY 14456-0462, USA

ABSTRACT

Center temperature–time profile of a 3·5% cornstarch dispersion heated in a vertical 303 × 404 can at 121°C compared favorably with finite element-based calculations with FIDAP computer simulation program. A thermo-rheological model based on experimental rheological data during starch gelatinization at 65–95°C and combined with an assumed submodel for decreasing viscosity at 95–121°C was used in the simulation. Most of the deviation between experimental and calculated profiles was about 5%, but a higher deviation (20%) occurred at the beginning of the heating cycle was attributed to higher heating rates $\sim 14°C\,min^{-1}$ than the $3°C\,min^{-1}$ used in gathering rheological data, and to settling of starch granules. The deviation from experimental data was higher when the decreasing segment of the η_a versus temperature data were omitted in the simulation. Shear rates that were high early during heating decreased due to increase in apparent viscosity (η_a) as a result of starch gelatinization. With heating, initially the velocity boundary layer was displaced away from the wall due to increase in the magnitudes of η_a of the STD close to the wall and subsequently moved closer to the wall due to decrease in η_a. Transient isotherms changed from Benard convection cells initially to stratified lines with increasing temperatures towards the top. © 1998 Elsevier Science Limited. All rights reserved

NOTATION

C	Constant, $C' = C^{-1}$
c_p	Heat capacity (kJ kg^{-1} K^{-1})
E_g	Activation energy of gelatinization (J mol^{-1})
g	Acceleration due to gravity (m s^{-2})

*To whom correspondence should be addressed.

G' Storage modulus (Pa)
G'' Loss modulus (Pa)

Gr   Grashof number, $\dfrac{gL^3\rho^2\beta\Delta T}{\eta^2}$ (dimensionless)

HT   Heating time (s)
k Thermal conductivity ($J\,s^{-1}\,m^{-1}\,K^{-1}$), reaction transmission coefficient, $(K\,s)^{-1}$
L Height of can (m)
p Pressure
r Distance in radial direction
R Gas constant ($8\cdot314\,J\,mol^{-1}\,K^{-1}$); radius of can
RT   Retort temperature (°C)
STD   Starch dispersion
t Time (s)
T Temperature of fluid (°C)
TR   Thermo-rheological
T_r Reference temperature
u Velocity in vertical direction
v Velocity in radial direction

Greek letters

α Shift factor, $\alpha' = \alpha^{-1}$
β Coefficient of thermal expansion (K^{-1})
λ Penalty parameter
η_a Apparent viscosity (Pa s)
η_{DIM} Dimensionless apparent viscosity
η^* Complex viscosity (Pa s)
η_{ug} Ungelatinized apparent viscosity (Pa s)
η_∞ Highest magnitude of η_a during gelatinization
ψ Integral of time–temperature history
ρ Density ($kg\,m^{-3}$)
$\dot{\gamma}$ Shear rate (s^{-1})
ω Frequency ($rad\,s^{-1}$)

INTRODUCTION

Starch is a common ingredient in many foods whose primary function is to provide thickening as a result of its gelatinization. In many foods, such as soups, salad dressings, gravies, and sauces, it is present in excess water. Because of the drastic increase in magnitude of the apparent viscosity (η_a), the rheological behavior of starch in excess water during the transition from fluid-like to viscoelastic behavior affects heat transfer during food thermal processing. Most models of starch gelatinization were developed under isothermal conditions, based on apparent first-order kinetics and the Arrhenius equation to describe the effect of temperature on the gelatinization rate (Kubota *et al.*, 1979; Lund, 1984; Lee *et al.*, 1984; Burros *et al.*, 1987; Dolan & Steffe, 1990; Okechukwu *et al.*, 1991; Kokini *et al.*, 1992; Okechukwu

& Rao, 1995). Because of the temperature history imposed during thermal processing, parameters obtained under isothermal conditions may not be suitable to describe changes in the apparent viscosity during gelatinization.

A comprehensive thermo-rheological (TR) model considering the effect of time–temperature history was developed by Dolan *et al.* (1989). Because it was discussed in detail by Yang and Rao (1998), it will not be discussed here. Yang and Rao (1998) studied the independent effect of heating rate, temperature, and ω on the behavior of η^* during gelatinization of 8% STDs, and correlation with steady shear parameters: (1) at a specific ω, temperature was the main factor that described changes in the η^* and the effect of heating rate was negligible for the rates, 1·6–6·0°C min^{-1}, and (2) the influence of ω on η^* was described by a shift factor based on a reference frequency (ω_r). The modified Cox–Merz rule (eqn (1)) was used to determine the parameters relating the dynamic and steady shear data, and a TR model for apparent viscosity was derived (eqn (2)).

$$\eta^*(\omega) = C[\eta(\dot{\gamma})]^x|_{\omega = \dot{\gamma}} \tag{1}$$

$$\eta_a = \left[C'\eta^*(T)\left(\frac{\dot{\gamma}_r}{\dot{\gamma}} \right) \right]^{x'} \tag{2}$$

where η^* is complex viscosity (Pa s) at frequency ω (rad s^{-1}), η_a is apparent viscosity (Pa s) at ($\dot{\gamma}$) shear rate (s^{-1}), C is a constant, α is the shift factor, C' is C^{-1}, α' is α^{-1}, $\dot{\gamma}$ is shear rate, $\dot{\gamma}_r$ is the reference shear rate, and η^* (T) is experimental complex viscosity data expressed as either a polynomial or a modified Oswin function, and temperature (T) is the independent variable. Equation (2) is a convenient TR model to numerically simulate thermal and other food processing problems.

Teixeira *et al.* (1969) and Manson (1971) applied finite difference methods to solve conduction heat transfer in cans. Datta and Teixeira (1988) numerically predicted transient temperature and velocity profiles of water-like canned food heated in a still retort; the slowest heating zone was a donut-shaped region near the bottom at about one-tenth the container height. Engelman and Sani (1983) used the finite element method to simulate pasteurization of bottled beer. Kumar *et al.* (1990) used the finite element method to simulate heating of non-Newtonian liquid foods in cans; the Arrhenius equation was used to express the influence of temperature on the apparent viscosity and the shear rate was considered to be constant at 0·01 s^{-1}. Their numerical results showed that the slowest heating point moved to the bottom center due to natural convection.

In foods containing starch, the η_a can increase significantly with temperature after the initial temperature of gelatinization is achieved. Ball and Olson (1957) associated viscosity data of corn starch dispersions with broken heating heat penetration data, but a direct correlation with starch gelatinization was not established because the data were obtained at a constant 60°C (140°F) with a Scott orifice viscometer. Stevens (1972) investigated broken heating phenomena; due to limited computer capabilities, complete numerical simulation was not conducted.

Although reliable TR data were obtained on 8% STDs (Yang & Rao, 1998), these dispersions did not show natural convection and broken heating curves; therefore, 3·5% STDs were used. The objectives of this study were to: (1) establish a functional TR model for η_a during gelatinization of 3·5% STDs based in part on eqn

(2) (Yang & Rao, 1998), (2) verify the applicability of the TR model by comparing the temperature–time profile from FIDAP numerical simulation of heat transfer to a 3·5% STD in a vertical 303 × 404 can with corresponding profile obtained from heat penetration data in a still retort, and (3) examine the characteristics of the predicted velocity and thermal boundary layers.

MATERIALS AND METHODS

Corn STDs

An unmodified corn starch (Cerestar USA, Hammond, IN) with the specifications: 10·0% moisture, 5·5 pH, and 99·5% granulation through US 200 mesh was used. Weighed amount of starch granules were mixed with distilled water and held over-night ($\sim$16 h) to allow starch hydration. In order to avoid settling of granules in the can during thermal processing, the 3·5% (w/w) STDs were pre-heated at 75°C for 5 min.

Rheological data

A rheometer (Carri–Med CSL-100, TA Instruments, New Castle, DE) was used to obtain dynamic rheological data with a 4 cm dia. parallel plate, gap of 500 μm (Yang & Rao, 1998) as the raw and pre-heated samples of 3·5% STDs were heated from 65 to 95°C in 10 min at 3·14, 12·57, and 47·12 rad s^{-1}. The magnitudes of η^* were computed by the rheometer software. Steady shear and frequency sweep (in the linear viscoelastic range) data on 3·5% (w/w) gelatinized STD were also obtained at 25°C with the rheometer using shear rates ($\dot{\gamma}$) in the same range as the frequencies (ω).

Numerical solution

Because of axisymmetry, heat transfer in a cylindrical container was considerably simplified to a two-dimensional problem. The governing partial differential equations were:

$$\text{The energy equation: } \rho c_\text{p}\left(\frac{\partial T}{\partial t} + v\frac{\partial T}{\partial r} + u\frac{\partial T}{\partial z}\right) = \frac{1}{r}\frac{\partial}{\partial r}\left(kr\frac{\partial T}{\partial r}\right) + \frac{\partial}{\partial z}\left(k\frac{\partial T}{\partial z}\right)$$

$$(3)$$

Because the STD exhibits viscoelastic behavior only after the initial gelatinization temperature is reached, the problem can not be approximated to simple heat trans-fer by conduction. In order to simplify the buoyancy force caused by density variation with temperature, Boussinesq approximation (eqn (4)) was used in the body force term of the momentum (eqn (5)) in the vertical direction:

$$\rho_\circ - \rho = \rho\beta(T - T_\circ) \tag{4}$$

$$\rho\left(\frac{\partial u}{\partial t} + u\frac{\partial u}{\partial z} + v\frac{\partial u}{\partial r}\right) = -\frac{\partial p}{\partial z} + \frac{1}{r}\frac{\partial}{\partial r}\left[r\eta\left(\frac{\partial u}{\partial r} + \frac{\partial v}{\partial z}\right)\right] + 2\frac{\partial}{\partial z}\left(\eta\frac{\partial u}{\partial z}\right)$$
$$+ \rho g[1 - \beta(T - T_r)] \tag{5}$$

The momentum equation in the radial direction is:

$$\rho\left(\frac{\partial v}{\partial t} + u\frac{\partial v}{\partial z} + v\frac{\partial v}{\partial r}\right) = -\frac{\partial p}{\partial z} + \frac{\partial}{\partial z}\left[\eta\left(\frac{\partial u}{\partial r} + \frac{\partial v}{\partial z}\right)\right] + \frac{2}{r}\frac{\partial}{\partial r}\left(r\eta\frac{\partial v}{\partial r}\right) - 2\eta\frac{v}{r^2} \tag{6}$$

The continuity equation is:

$$\frac{1}{r}\frac{\partial(r\rho v)}{\partial r} + \frac{\partial(\rho u)}{\partial z} = 0 \tag{7}$$

Heat transfer to a 303×406 can with: $R = 4.2$ cm and $L = 10.7$ cm, and no head space was studied. The boundary conditions for solving the equations were (see Fig. 1): (1) wall at $r = R$, $0 \leq z \leq L$, $T = RT$, $u = 0$ and $v = 0$, (2) top wall at $z = L$, $0 \leq r \leq R$, $T = RT$, $u = 0$ and $v = 0$, (3) bottom wall at $z = 0$, $0 \leq r \leq R$, $T = RT$, $u = 0$ and $v = 0$, and (4) axisymmetric line at $r = 0$, $0 \leq z \leq L$, $\partial T/\partial r = 0$, $\partial u/\partial r = 0$ and $v = 0$. The initial conditions were: $0 \leq r \leq R$, $0 \leq z \leq L$, $T = IT$, $u = 0$ and $v = 0$. Since the magnitude of η_a during gelatinization could be from 10 to 2000 times higher than that of ungelatinized STD, the changes in the other fluid properties with the temperature were neglected, and were assumed to be equal to those of water: $\rho = 1000$ kg m^{-3}, $c_p = 4.18$ kJ kg^{-1} K^{-1}, $k = 0.66$ J s^{-1} m^{-1} K^{-1}, and $\beta = 0.0005$ K^{-1} at 70°C.

The governing equations with conditions described above were solved with FIDAP fluid dynamics analysis program (Version 7.5, Fluid Dynamics International, Inc., Evanston, IL) on a Gateway 2000 computer platform (P5-100, Intel Pentium 32MB RAM, North Sioux City, SD). FIDAP is based on the finite element method for simulating fluid flow, and heat and mass transfer problems (Engelman & Sani, 1983; Engelman, 1993; Dhatt & Touzot, 1984; Engelman, 1993). In the finite element method, the continuum region of study is divided into a number of shaped elements and the method of weighted residuals with Galerkin's criteria is used to reduce the errors resulting from the approximation of the velocity, pressure and temperature fields within each element. The penalty approach (eqn (8)) was used to replace the continuity equation, eliminating the unknown pressure, and thus simplifying solution of the problem.

$$\frac{1}{r}\frac{\partial(r\rho v)}{\partial r} + \frac{\partial(\rho u)}{\partial z} = -\frac{1}{\lambda}p \tag{8}$$

where λ is the penalty parameter with a magnitude range of 10^5–10^8. Because λ is very large, there is no significant loss of accuracy when the original equation is replaced by the eqn (8). An implicit time integration (backward Euler) with variable time increment was used to study the transient behavior. At each time step, the nonlinear system was solved by the quasi-Newton procedure. This method was

chosen over the other Newton-type algorithms because the form of Jacobian matrix that is recomputed and updated reduces considerably the computer time (Engelman & Sani, 1983).

Our preliminary effort to verify the capability of FIDAP was to simulate the more difficult study of Datta and Teixeira (1988) because of the highest Gr number, $\sim 10^{10}$, while in our problem, the Gr number was much lower, $\sim 10^6$, and closer to the magnitude $\sim 10^5$ in Engelman and Sani (1983). The PC was dedicated entirely for this study, allowing us to try different mesh densities, and solution strategies offered by FIDAP, including: successive substitution, Newton–Raphson, and quasi-Newton, different values of penalty parameter, relative error, residual vector, relaxation factor, number of iterations allowed by time step, transient algorithms, and different values for the streamline upwind scheme. The initial guidelines for FIDAP were based on the study of Engelman and Sani (1983). The convergence at

Fig. 1. Finite element mesh of #303 can used in numerical simulation.

each time step could be monitored by a graph on the screen/monitor which allowed us to change the strategy in the early stage of simulation. We found that the FIDAP results were closer to that of Datta and Teixeira (1988) when the mesh density near the wall was increased, as expected, and when the value of the streamline upwind scheme was decreased.

In order to verify the effect of mesh density on our results, we even simulated the problem with a non-uniform mesh with up to 100 nodal points in each direction which required more than five days CPU to simulate the first 10 s of heating. Only when our calculated velocity and temperature profiles, and flow patterns were comparable with those shown in Datta and Teixeira (1988), we simulated our problem. One of the FIDAP options allowed us to use fixed time increment $(1 \times 10^{-5}$ s) at a certain number of initial steps when the initial temperature differences were still very high. The simulation stopped if the convergence was not achieved after 10 successive time reductions in the time variable mode, which allowed us to restart at the time of interruption with a smaller time increment. The transient algorithms with variable time increment are well described in the study of Engelman and Sani (1983). The nodal points were successively reduced from the initial mesh to reduce the simulation time, but with the capability to resolve the problem identified by Datta and Teixeira (1988). Further, the temperature profiles were always checked with those of the previous mesh in order to not lose significant accuracy.

The results shown were obtained with a mesh of 2115 nine node isoparametric elements, 45 in the radial direction and 47 in the axial direction (Fig. 1). However, we may not have reached the ideal mesh density in terms of reducing the computer time because we judged that two to three days of running time was acceptable for our needs. For comparison, Engelman and Sani (1983) used a mesh consisting of 310 isoparametric elements, 10 in the radial direction and 31 in the axial direction, and in their finite difference-based study (Datta & Teixeira, 1988), used a grid of 39×39 to form the non-uniform grid.

Magnitudes of shear rate were determined by computing the components of the strain rate tensor (eqns (9) and (10)).

$$\dot{\gamma}_{ij} = \begin{pmatrix} \dfrac{\partial u}{\partial x} & \dfrac{1}{2}\left(\dfrac{\partial u}{\partial y} + \dfrac{\partial v}{\partial x} \right) \\ \dfrac{1}{2}\left(\dfrac{\partial v}{\partial x} + \dfrac{\partial u}{\partial y} \right) & \dfrac{\partial v}{\partial y} \end{pmatrix} \tag{9}$$

$$\dot{\gamma} = (\dot{\gamma}_{ij}\dot{\gamma}_{ij})^{\frac{1}{2}} \tag{10}$$

where $\dot{\gamma}$ is shear rate, $\dot{\gamma}_{ij}$ is the strain rate tensor, and i and j are x and y coordinate directions, respectively. Additional assumptions in the TR model and numerical solution were:

(1) due to the low starch concentration, up to 78°C the STD behaved like a Newtonian fluid with magnitude of the viscosity constant at 0·001 Pa s.

(2) The parameters of the correlation between η^* and η_a did not change with temperature during the gelatinization process. Although the modified Cox–Merz rule has been shown to be valid for fully gelatinized STDs that

exhibited shear-thinning behavior, shear thickening behavior was observed during the early stages of gelatinization (Bagley & Christianson, 1982; Christianson & Bagley, 1983, Okechukwu & Rao, 1995). At the beginning of gelatinization, the value of the η_a is so low ($\sim 10^{-3}$ Pa s) (Okechukwu & Rao, 1995) compared with that at the final stage of gelatinization, that an error due to the Cox–Merz correlation would not affect significantly the numerical results.

(3) The thermal resistance of the can's metal wall was neglected and the temperature boundary condition imposed on the side wall, top, and bottom was the retort temperature obtained from the heat penetration data.

(4) The proposed model of viscosity was independent of heating rate (Yang & Rao, 1998) for a restricted range of heating rates.

Heat penetration tests

Commercial 303×406 cans were completely filled with either raw or pre-heated 3·5% (w/w) STDs. Copper-constantan thermocouples (Type CNS, Ecklund Custom Thermocouples, Cape Coral, FL) were used to measure the temperature at the geometric center of each can. CALSoft II software and a CALPlex data logger (TechniCAL, Inc., New Orleans, LA) were used with a computer (Gateway 2000, P5-75) to obtain and store the time–temperature data at 10 s intervals. The thermocouples were calibrated at the boiling temperature of water at normal atmospheric pressure. The filled cans were seamed just before each run to minimize settling of starch granules and heated in the upright position on a rack built of thin wire to ensure bottom heating in a pilot scale still retort. In each run, temperatures in at least two cans were monitored. Saturated steam at 121°C was used as the heating medium and the heating cycle was terminated when the center temperature was within about 1·5°C of the retort temperature. Data from the cooling cycle was not considered.

RESULTS AND DISCUSSION

Rheological data

In contrast to data of 6% and 8% STDs, at the lower 3·5% starch concentration, the values of complex viscosity, particularly in the early stage of gelatinization, did not produce an acceptable response waveform until $T \geq 78°C$. Experiments conducted at 47·12 rad s^{-1} could not be reproduced, very likely because structure formation during gelatinization was affected at the low starch concentration. Frequencies <3·14 rad s^{-1} were tried, but the data were not considered because of excessive rheometer noise. For the numerical simulations, magnitudes of the viscosity at 3·14 rad s^{-1} were considered to be the highest values possible during heating and assumed to be nearly equal to the limiting viscosity at zero shear rate. The viscosities of raw and pre-heated STDs were not different, probably because of low STD concentration and mild pre-heating (5 min at 75°C). Magnitudes of η^* at 3·14 rad s^{-1} and 12·57 rad s^{-1} were superposed to 3·14 rad s^{-1} as described by Yang & Rao (1998).

Experimental TR data were averaged and the results used to fit submodels for simulation as shown in Fig. 2. The increasing segment (A–B) of the η^* curve that was sigmoid shaped was fitted to a modified Oswin model (eqn (11)):

$$\eta^*\left(\frac{\omega}{\omega_r}\right) = 7\cdot4 \times 10^{-6\cdot0}\left(\frac{T}{100-T}\right)^{6\cdot208} ; \; R^2 = 0\cdot99 \tag{11}$$

The segment (B–C) from 89·5°C to 92·5°C, that contained the end of increase in viscosity section, the peak viscosity value, and beginning of the decreasing part of the viscosity curve was well described by a third order polynomial (eqn (12)).

$$\eta^*\left(\frac{\omega}{\omega_r}\right) = -69122\cdot86 + 2244\cdot36T - 24\cdot28T^2 + 0\cdot088T^3; \; R^2 = 0\cdot99 \tag{12}$$

It is emphasized that rheological data described by eqns (11) and (12) of a STD cannot be predicted a priori and must be obtained experimentally. Because viscosities at ≥ 95°C were severely affected by water evaporation in our rheometer, two possible profiles were tested for temperatures from 95°C to 121°C (retort tempera-
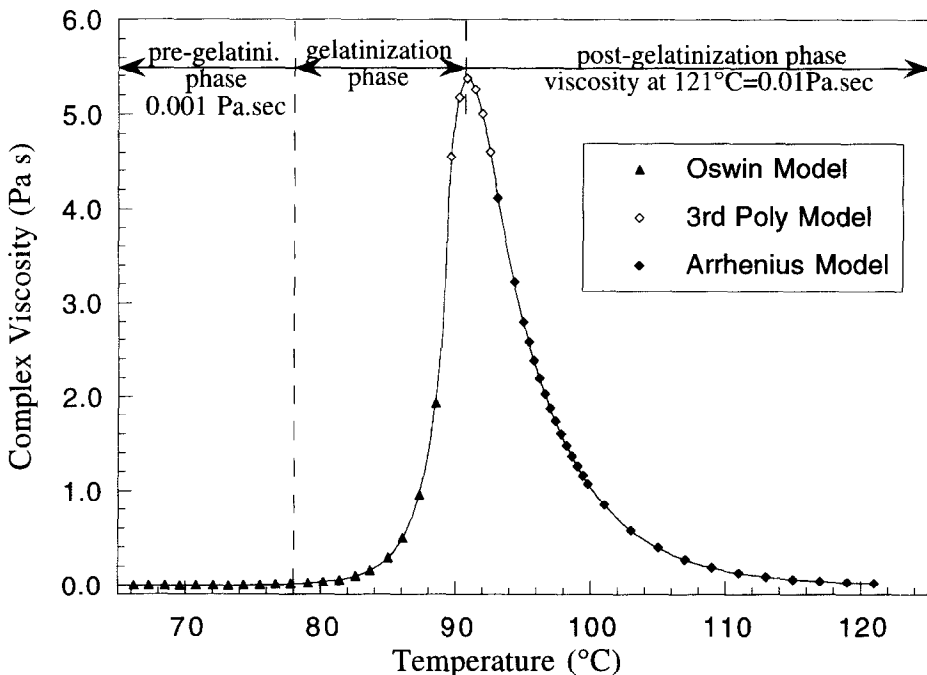
Fig. 2. Complex viscosity–temperature master curve of 3·5% corn starch dispersion described by three submodels. Oswin, third-order polynomial, and Arrhenius.

ture) (C–D): (1) that the values of η^* decreased up to 95°C, at which the last measurement was recorded, as shown by the experimental results and then the rate of decrease was so slow that it could be considered to be constant (Yang & Rao, 1998), and (2) that decrease in magnitudes of the η^* with increase in temperature was described by an Arrhenius equation (eqn (13)).

$$\eta^*\left(\frac{\omega}{\omega_r}\right) = 4 \cdot 11\exp\left[\frac{227 \cdot 1 \times 10^3}{R}\left(\frac{1}{T} - \frac{1}{366 \cdot 1}\right)\right]; \ R^2 = 0 \cdot 97 \qquad (13)$$

Because of the availability of reliable TR data from 65°C to 95°C during gelatinization (eqns (11) and (12)), as well as of both the experimental heat penetration data and computer simulation based temperatures, it was considered safe to assume the temperature profile described by eqn (13) from 95°C to 121°C. Comparison of the numerically calculated temperatures with the experimental profiles to be discussed strongly support the assumption of an Arrhenius model (eqn (13)) for the magnitudes of η_a from 95°C to 121°C.

In eqn (13), the reference temperature 366·1 K was the mean value of temperatures of the decreasing segment of η^*. The value of E_a in eqn (13) determined to be 227·1 kJ mol^{-1} is higher compared to those reported for gelatinized corn starch at lower temperatures. Given the large decrease in viscosity, the value of E_a is reasonable and it is in good agreement with the value of $E_g = 240$ kJ mol^{-1} in the model of Dolan et al. (1989) for the increasing viscosity segment (Yang & Rao, 1998). There is a difference between the decrease in viscosity with increasing temperature that occurs just after the peak viscosity has been reached and the decrease in viscosity with temperature that occurs in cooled gelatinized STDs. For instance, for the same STD sample after it was heated up to 95°C and cooled to 25°C, the value of $E_a = 14 \cdot 5$ kJ mol^{-1} was determined from the viscosities measured at 35°C and 75°C. Based on the modified Cox–Merz rule (Fig. 3), the constant C and shift factor α found were 2·07 and 1·01 at 25°C, respectively.

Numerical simulation scenarios

Based on eqns (11)–(13), and Cox–Merz rule parameters, three user-supplied subroutines of the following scenarios were developed: (1) a complete TR model that included the effect of shear rate and decrease in the value of η_a with temperature after the peak viscosity described by an Arrhenius equation (COM), (2) a no shear TR model similar to the previous one, but with a constant shear rate 3·14 rad s^{-1} (NSM), and (3) a peak viscosity TR model that included the effect of shear rate, but assumed the value of η_a to be constant after 95°C (PVM). The applicable subroutine was called once for each boundary and continuum element in the mesh and returned the values of the η_a at each time step.

Calculated and experimental center temperatures

The numerically predicted transient temperatures for the three TR model scenarios and the experimental heat penetration data at the center of the can are shown in Fig. 4. The results showed that the overall predicted transient temperatures for the

COM and NSM models were in good agreement with the experimental data. Although the predicted temperatures from the PVM model followed the same shape as the experimental data, they were considerably lower than the experimental values. The higher temperatures predicted by the COM and NSM models suggest that the assumption of a continually decreasing viscosity profile after 95°C was realistic. Based on eqn (13), the value of η_a decreased drastically from the peak value of 2·6–0·01 Pa s at 121°C that was still ten times higher than the value of 0·001 Pa s prior to initiation of gelatinization.

During the first 500 s of heating (Fig. 5), except in the range 40–100 s where the difference between the predicted and experimental data was around 20%, most of the predicted data deviated by less than 5%. The observed difference in the range 40–100 s may be due mainly to: (1) although pre-heating of the STD reduced settling of starch granules, some settling still occurred during heating that lowered the starch concentration in main core of the STD, and (2) the heating rate (3°C min^{-1}) used to obtain TR data was lower than the average heating rates of about 14°C min^{-1} at the beginning of heating near the wall, where the boundary layer developed. Yang and Rao (1998) found a maximum difference of about 25% in peak viscosity values at the heating rates 6·0°C min^{-1} and 1·6°C min^{-1}. With our rheometer, because a temperature sweep from 65°C to 95°C would have to be performed in about 2 min, it would not be possible to obtain accurate data at the heating rate of 14°C min^{-1}. In this short time span, the rheometer would not
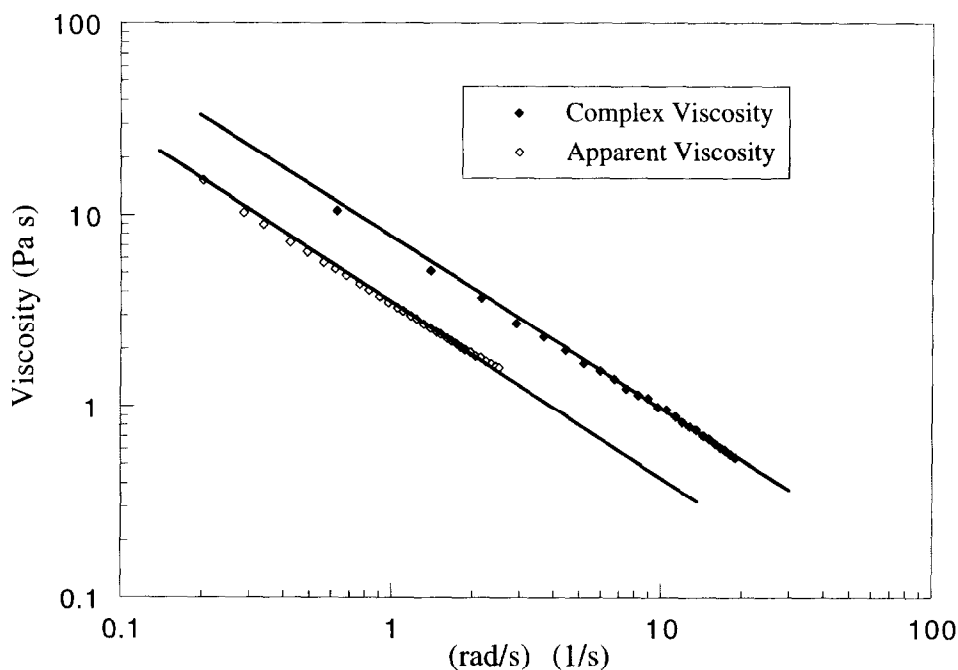
Fig. 3. Complex viscosity versus oscillatory frequency and apparent viscosity versus shear rate data of 3·5% corn starch dispersion at 25°C.

acquire enough data to describe accurately the TR behavior and because of the response time of the rheometer, there would be errors in measurement of the rapidly changing temperature. However, because of the low magnitudes of strains applied to the sample, dynamic rheological tests are well suited for obtaining TR data and the low values of strains are very appropriate for natural convection heating of STDs in cans.

A small negative difference of less than 5% during the later stages of heating may be due to either neglecting the thermal resistance of the can's wall or due to the magnitudes of η_a at this stage being slightly higher than those predicted by eqn (13). Considering that both TR and heat penetration experiments with STDs require considerable care, the agreement between the experimental and the calculated COM and NSM temperature profiles is a positive development.

Effect of shear rate on center temperatures
The effect of shear rate on the center point heating rate can be also seen in Fig. 5. The COM model prediction which included both the effect of shear rate and the Arrhenius equation to describe the decrease of the magnitudes of η_a with temperature was slightly closer to the experimental curve than that of the NSM model. In this study, it also appears that because of increase in viscosity due to gelatinization,
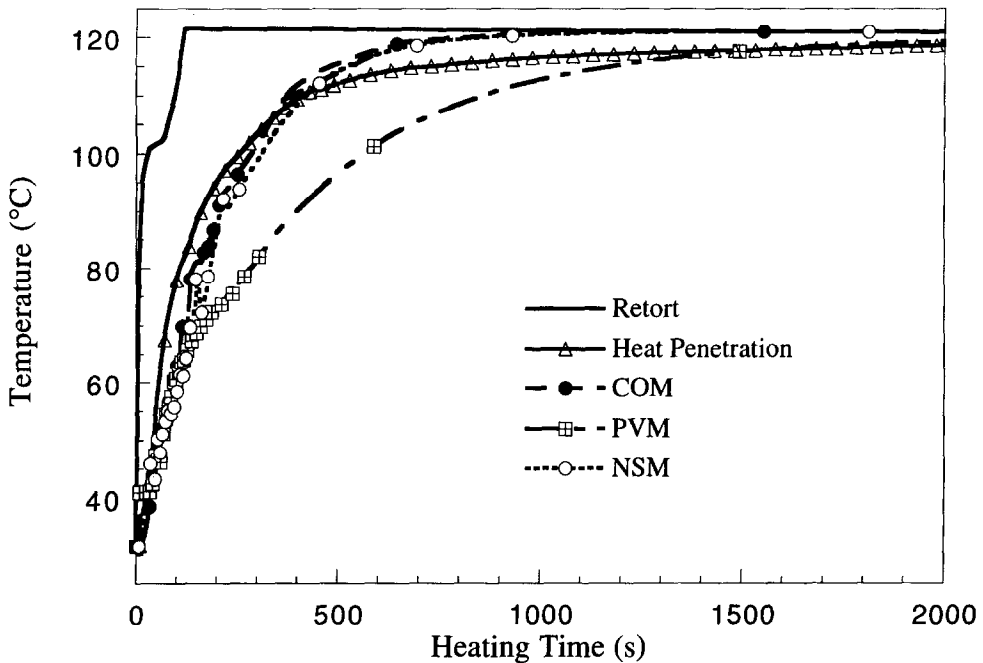
Fig. 4. Experimental and predicted heating curves at the center of the can considering the three thermo-rheological scenarios: COM model accounts for both shear and temperature, NSM model accounts for temperature but assumes a constant shear rate $3{\cdot}14\,\mathrm{rad\,s^{-1}}$, and PVM model assumes that after peak value is reached viscosity remains constant at that value.

the shear rate effects we not significant. Although the effect of shear rate contributed to some improvement in heat transfer, the temperatures at the center predicted by both models were not significantly different. Because the velocities developed due to the natural convection were low, the shear rates were neglected in other studies (Stevens, 1972; Kumar *et al.*, 1990). However, for fluids whose viscosities decrease with shear rate and temperature, velocity gradients in strong boundary layers will reduce the magnitudes of η_a and consequently affect heat transfer rates.

Simulated boundary layers

Effect of shear rate in model
The effect of shear rate on η_a and axial velocity at a point 0·5 mm from the wall in the boundary layer at mid-height of the can predicted by the COM and NSM models over the first 250 s of heating time (HT) is shown in Fig. 6. Shear rate-heating time profiles were (not shown) similar to those of axial velocities.

(1) At the beginning of heating, because the viscosity was similar to that of water, the increase in velocity and the development of the velocity boundary layer were similar to those of a water-like product (Datta & Teixeira, 1988). The shear rate was as high as $50\,s^{-1}$, but because the STD was a Newtonian fluid at this stage, there was no effect on the magnitudes of η_a.
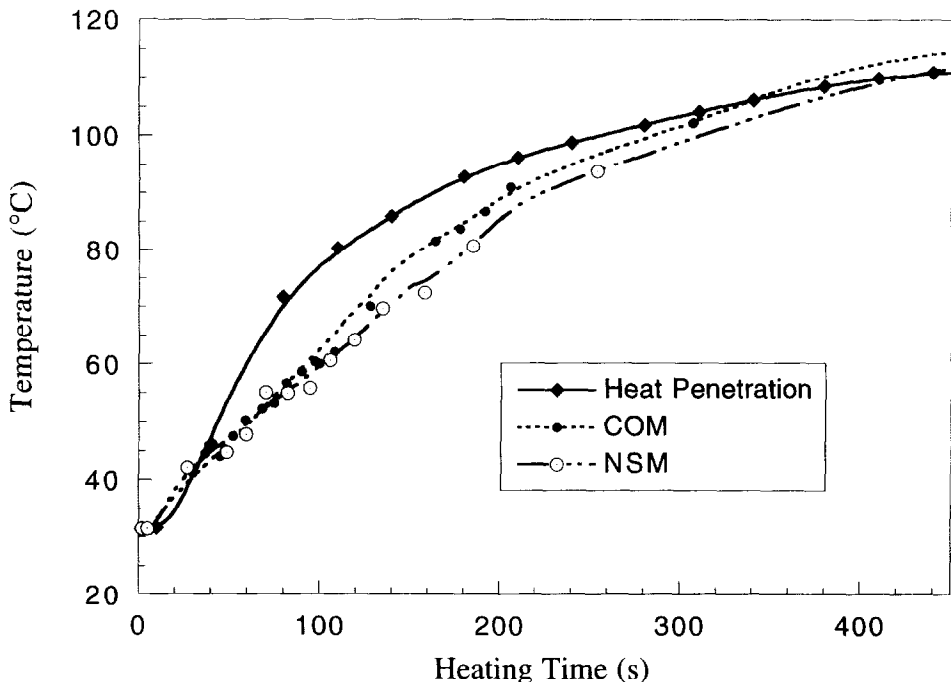
Fig. 5. Experimental and predicted heating curves at the center of the can during the first 500 s of heating.
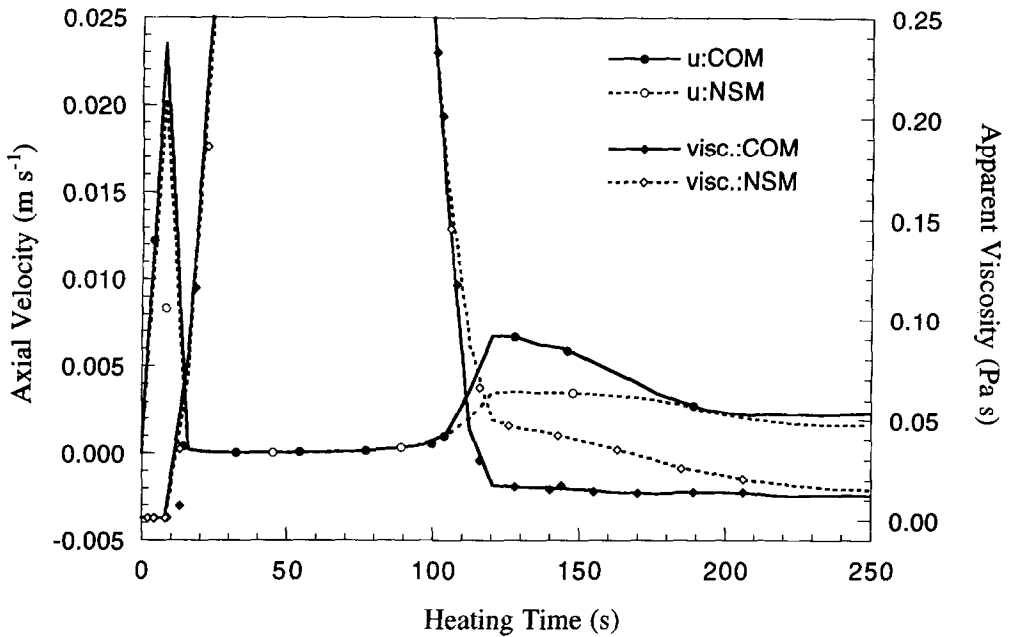
Fig. 6. Axial velocity and apparent viscosity history 0·5 mm from the wall at mid-height of the can.

(2) As HT increased, once the initial temperature of gelatinization was reached, the viscous forces became predominant and magnitude of the axial velocity decreased practically to zero in a few seconds. The heat transfer mode was conduction during the entire gelatinization phase and part of the post-gelatinization phase when η_a started to decrease but was still high. Also, there was no significant difference between the predictions of the COM and NSM models because the shear rate was so low that the reference shear rate was assumed in the COM model. The shear rate dropped to almost zero, and again there was not much effect on the magnitudes of η_a because it was below the cut off shear rate of the subroutine.

(3) As the heating was continued, η_a decreased according to the Arrhenius model to values where the buoyancy forces increased the magnitude of the axial velocity and the effect of shear rate again became evident. In Fig. 6, values of η_a above 0·25 Pa s were excluded in order to show the difference between the magnitudes of η_a for both models. In the range of HTs 100–180 s, the reduction in η_a and the resulting increase in axial velocity due to the increase in shear rate to about 12 s^{-1} were more evident for the COM model than for the NSM model.

COM model velocity and thermal boundary layers

In order to better understand transient heat transfer phenomena, the velocity and thermal boundary layers, and the corresponding η_a at mid height in the can were

tracked at HTs. At HT 5 s (Fig. 7, top), the buoyancy force created by the difference in temperature moved the STD fluid upward, reaching the highest velocities near the wall. Because the temperature difference was not high, $\sim 30°C$, the small recirculation of the fluid resulted in low negative velocities. Since there were no major changes in viscosity at this heating time, the axial velocity and temperature profiles were similar to those reported in other studies on natural convection heating of water-like fluids (Hiddink, 1975; Engelman & Sani, 1983; Datta & Teixeira, 1988). At the HTs 25, 75 and 100 s (Fig. 7, top), the velocity boundary layer was displaced away from the wall due to increase in the magnitudes of η_a of the STD close to the wall. At the displacement location, the viscous forces increased the resistance to
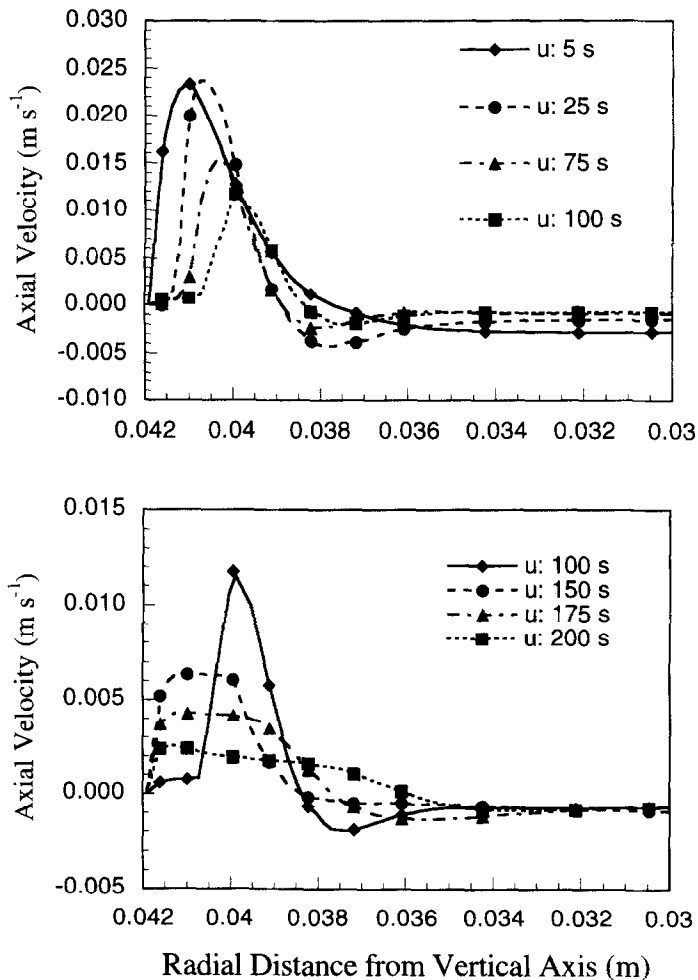
Fig. 7. Development of predicted velocity boundary layer with heating times, (a) 5, 25, 75, and 100 s, and (b) 100, 150, 175, and 200 s.

flow and reduced the velocity to almost zero. As the heating progressed from 25 to 100 s, the width of the displacement increased since the gelatinization progressed to that region. Except for decrease in maximum positive velocity with heating time as a result of the decrease in difference in temperatures, the velocity profiles after the displacement looked similar to that at HT 5 s. The maximum positive velocity, 25 mm s^{-1} at 25 s, in this study was about the same reported by others: 35 mm s^{-1} at 30 s by Datta (1986), and 32 mm s^{-1} at 30 s observed by Hiddink (1975).

At HTs 150, 175, and 200 s (Fig. 7, bottom), the magnitudes of η_a were sufficiently low so that in relation to viscous forces the buoyancy forces were high enough to promote the axial velocity profile near the wall. As expected, the thickness of the
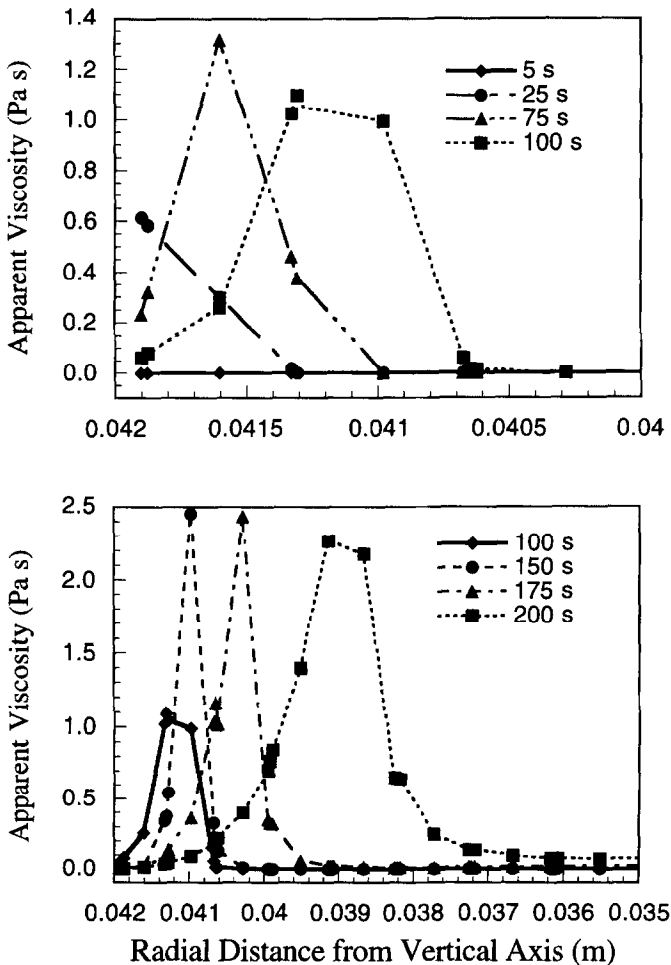
Fig. 8. Development of predicted apparent viscosity with heating times, (a) 5, 25, 75, and 100 s, and (b) 100, 150, 175, and 200 s.

velocity boundary layer increased with time due to gelatinization caused by penetration of heat. However, the downward velocity curve was marked by a section where the magnitudes of axial velocity decreased at a slower rate. In this section, the resistance to flow increased because of increase in the magnitude of η_a and the length of this section corresponded to the radial distance where the magnitudes of η_a were large (Fig. 8).

In comparison to the velocity and viscosity profiles, the thermal boundary layer history (Fig. 9) was simpler; compared to the temperature–radial distance profile at 100 s, there was a large increase at 150 s after the transition to the post-gelatinization phase.
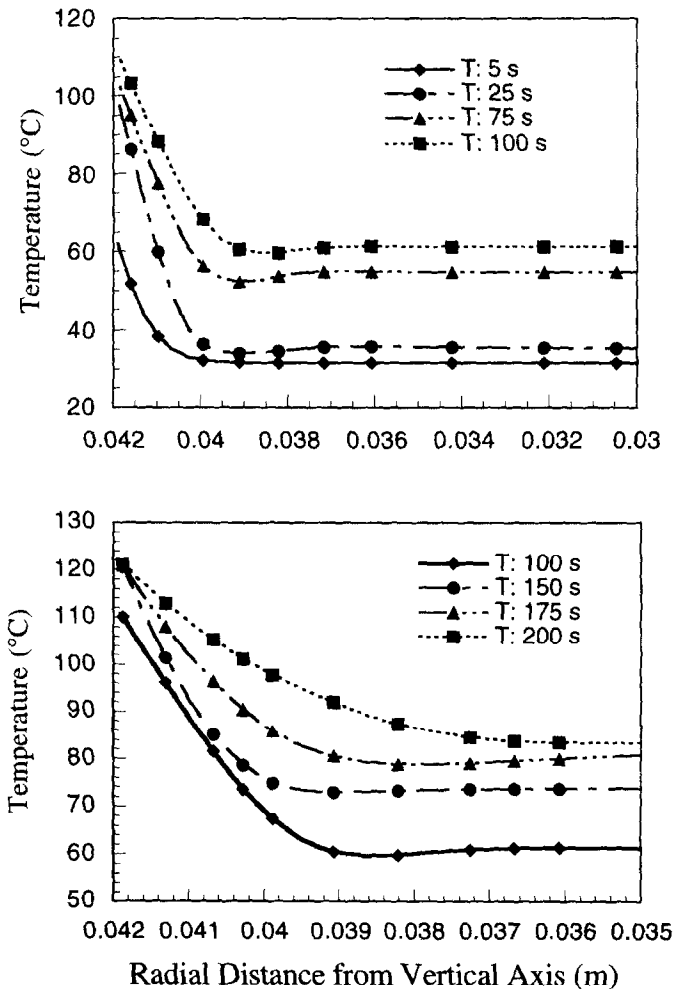
Fig. 9. Development of predicted thermal boundary layers with heating times, (a) 5, 25, 75, and 100 s, and (b) 100, 150, 175, and 200 s.

Detailed description of the transient isotherms and apparent viscosity contours in the left side of the can at the HTs 5, 25, 75, 100, 150, 175, 200, 350, 750, and 1000 s were discussed by Yang (1997). Here, Figs 10 and 11 illustrate the transient isotherms at HTs 175 and 1000 s and apparent viscosity contours after 150 and 1000 s, respectively. At the beginning of heating (5 s), the isotherm was characterized by rise in velocity of hot STD along the side wall, which converged at the top, and by the presence of Benard convection cells near the bottom due to the bottom heating

After 175 s   After 1000 s
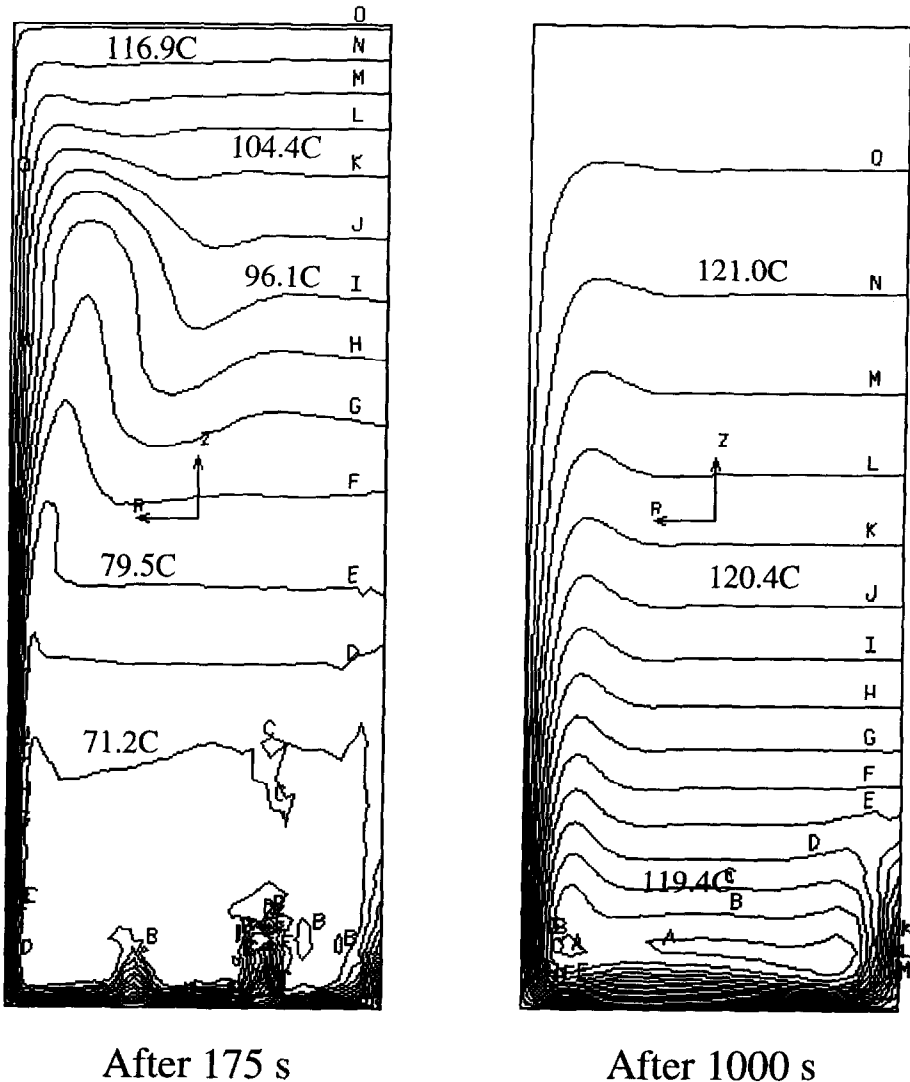
Fig. 10. Predicted isotherms in a cylindrical container after 175 and 1000 s of heating.

that were not as sharp as those reported by Datta and Teixeira (1988) because the come-up time was included in this study and thus the temperature difference was not that large. The η_a contour at 5 s was not presented because it had a constant value at this time. As the STD was heated to 25 and 75 s, the initial temperature of gelatinization was reached and a layer of gelatinized starch formed along the top

0.44 Pa s A

1.31 Pa s B

2.18 C

Viscosityafter 150 s

0.010 Pa s A

B

0.011 Pa s C

0.012 Pa s D

E
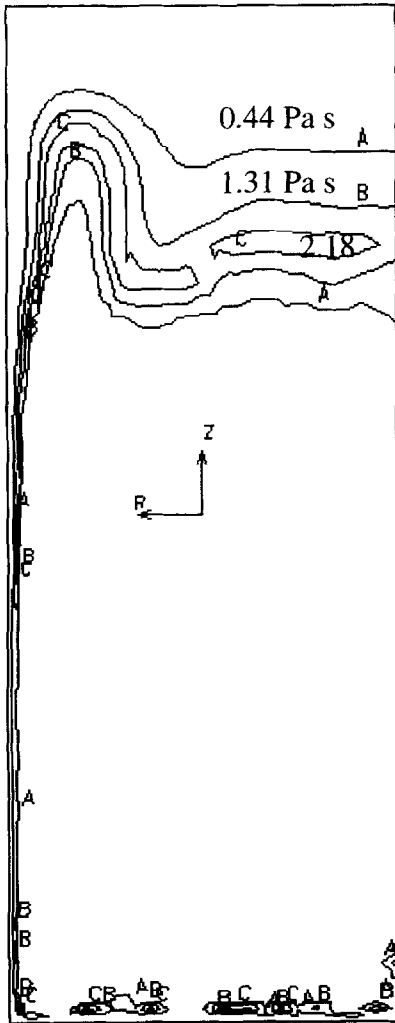
0.013 Pa s
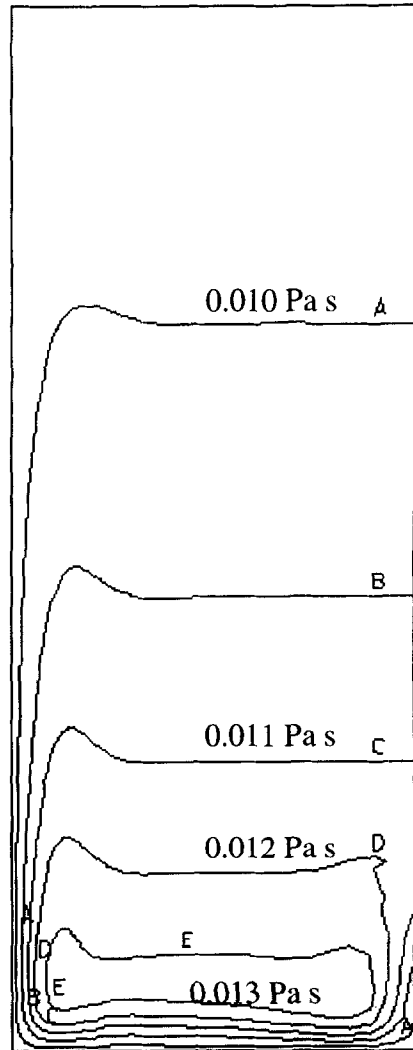
Viscosity after 1000 s

Fig. 11. Predicted apparent viscosity contour in a cylindrical container after 150 and 1000 s of heating.

wall, bottom and side wall. Because the highest temperature was at the top, the thickness of the gelatinized starch layer along the wall was also highest at the top and decreased from top to bottom. The convection cells near the bottom due to the bottom heating generated secondary loops. A counterclockwise loop (left side of the can) near the bottom forced the hot STD fluid upwards near the centerline, resulting in rise in temperature near the centerline and from the bottom.

As the HT increased (100, 150, 175 and 200 s), the temperature increased and the portion of gelatinized starch nearest the walls reached the post-gelatinization phase and lower magnitudes of η_a. The thickness of gelatinized starch grew according to the temperature profile. At this time, the isotherms near the top assumed characteristics of conduction heating without rises in temperature near the wall because of the dominant viscous forces. At HT 350 s, the temperatures at the bottom half of the can were close to the value at which the magnitude of η_a was the highest, therefore, eliminating most of the convection cells. However, a counterclockwise loop was still present since that region was hotter and therefore was already at the post-gelatinization phase. Because the STDs at the top half were in the late post-gelatinization phase, the buoyancy forces became dominant again. At 750 and 1000 s, the isotherms became very stratified with increasing temperatures towards the top. The thickness of the boundary layer at bottom half and at the side wall became more uniform because η_a was of the same order of magnitude.

CONCLUSIONS

There was good agreement between can center's experimental and calculated temperature–time profiles, so that the thermo-rheological model was satisfactory for describing shear and temperature effects as a 3.5% starch dispersion was heated. The maximum deviation in the temperature–time profiles of about 20% early during heating was due either to the very high heating rates or some settling of starch granules. The FIDAP simulation program can be a useful tool for studying transient natural convection heat transfer to foods provided that suitable physical and thermal property data are available; in particular, suitable thermo-rheological data are very important for obtaining meaningful results. The predicted velocity and temperature profiles reflected the changes in apparent viscosity that were in turn caused by temperature and shear during heating.

ACKNOWLEDGEMENTS

REFERENCES

Bagley, E.B. & Christianson, D.D. (1982). Swelling capacity of starch and its relationship to suspension viscosity: Effect of cooking time, temperature and concentration. *J. Texture Studies*, **13**, 115–126.

Ball, C. O. & Olson, F. C. W. (1957). *Sterilization in Food Technology*, 1st ed. McGraw Hill, New York.

Burros, B.C., Young, L.A. & Carroad, P.A. (1987). Kinetics of corn meal gelatinization at high temperature and low moisture. *J. Food Sci.*, **52**, 1372–1376, 1380.

Christianson, D.D. & Bagley, E.B. (1983). Apparent viscosities of dispersions of swollen cornstarch granules. *Cereal Chem.*, **60**, 116–121.

Datta, A. K. (1986). *Numerical modeling of natural convection and conduction heat transfer in canned foods with application to on-line process control*, University of Florida, Gainesville, FL.

Datta, A.K. & Teixeira, A.A. (1988). Numerically predicted transient temperature and velocity profiles during natural convection heating of canned liquid foods. *J. Food Science*, **53**, 191–195.

Dhatt, G. & Touzot, G. (1984). *The Finite Element Method Displayed*, 1st ed., John Wiley and Sons, New York.

Dolan, K.D. & Steffe, J.F. (1990). Modeling rheological behavior of gelatinizing starch solutions using mixer viscometry data. *J. Texture Studies*, **21**, 265–294.

Dolan, K.D., Steffe, J.F. & Morgan, R.G. (1989). Back extrusion and simulation of viscosity development during starch gelatinization. *J. Food Process Engineering*, **11**, 79–101.

Engelman, M. S. (1993). *FIDAP, Fluid Dynamics International, Inc.*, Evanston, IL.

Engelman, M.S. & Sani, R.L. (1983). Finite-element simulation of an in-package pasteurization process. *Numerical Heat Transfer*, **6**, 41–54.

Hiddink, J. (1975). Natural convection heating of liquids, with reference to sterilization of canned foods. *Agricultural Research Reports*, 839. Center for Agricultural Publishing and Documentation, Wageningen, Netherlands.

Kokini, J.L., Lai, L.S. & Chedid, L.L. (1992). Effect of starch structure on starch rheological properties. *Food Technology*, **46**, 124–139.

Kubota, K., Hosakawa, Y., Suzuki, K. & Hosaka, H. (1979). Studies on the gelatinization rate of rice and potato starches. *J. Food Science*, **44**, 1394–1397.

Kumar, A., Bhattacharya, M. & Blaylock, J. (1990). Numerical simulation of natural convection heating of canned thick viscous liquid food products. *J. Food Science*, **55**, 1403–1411, 1420.

Lee, S.Y., Cho, H.Y., Kim, S.K., Lee, S.K. & Pyun, Y.R. (1984). Rheological properties during gelatinization of rice starch. *Korean J. Food Sci. Technol.*, **16**, 273–278.

Lund, D.B. (1984). Influence of time, temperature, moisture, ingredients, and processing conditions on starch gelatinization. *Critical Reviews in Food Science and Nutrition*, **20**, 249–273.

Manson, J. E. (1971). Thermal process evaluation of conduction heating food in an anomalous shaped container. *Ph.D. Thesis*, Univ. of Massachusetts, Amherst, MA. *Dissertation Abstracts International*, Section B, vol. 32, p. 1518.

Okechukwu, P.E., Rao, M.A., Ngoddy, P.O. & McWatters, K.H. (1991). Flow behavior and gelatinization of cowpea flour and starch dispersions. *J. Food Science*, **56**, 1311–1315.

Okechukwu, P.E. & Rao, M.A. (1995). Influence of granule size on viscosity of cornstarch suspension. *J. Texture Studies*, **26**, 501–516.

Stevens, P. M. (1972). Lethality calculations, including effects of product movement, for convection heating and broken heating foods in still-cook retorts. *Ph.D. Thesis*, Univ. of Massachusetts, Amherst, MA.

Teixeira, A.A., Dixon, J.R., Zahradnik, J.W. & Zinsmeister, G.E. (1969). Computer optimization of nutrient retention in the thermal processing of conduction-heated foods. *Food Technology*, **23**, 137–142.

Yang, W. H. & Rao, M. A. (1998). Complex viscosity–temperature master curve of cornstarch dispersion during gelatinization. *J. Food Process Eng.*, in press.

Yang, W. H. 1997. Rheological behavior and heat transfer to a canned starch dispersion: computer simulation and experiment. *Ph.D. Thesis*, Cornell University, Ithaca, NY.